# Gas Plume Quantification in Downlooking Hyperspectral Longwave Infrared Images

Caroline S. Turcotte*[a], Michael R. Davenport[b]

[a]Defence Research and Development Canada (DRDC) - Valcartier, 2459 Pie-XI Blvd. North, Québec, Québec, CANADA, G3J-1X5;

[b]Salience Analytics Inc., 87 W 41 Ave, Vancouver, BC, CANADA, V5Y-2R8.

## ABSTRACT

Algorithms have been developed to support quantitative analysis of a gas plume using down-looking airborne hyperspectral long-wave infrared (LWIR) imagery. The resulting gas quantification "GQ" tool estimates the quantity of one or more gases at each pixel, and estimates uncertainty based on factors such as atmospheric transmittance, background clutter, and plume temperature contrast. GQ uses gas-insensitive segmentation algorithms to classify the background very precisely so that it can infer gas quantities from the differences between plume-bearing pixels and similar non-plume pixels. It also includes MODTRAN-based algorithms to iteratively assess various profiles of air temperature, water vapour, and ozone, and select the one that implies smooth emissivity curves for the (unknown) materials on the ground. GQ then uses a generalized least-squares (GLS) algorithm to simultaneously estimate the most likely mixture of background (terrain) material and foreground plume gases. Cross-linking of plume temperature to the estimated gas quantity is very non-linear, so the GLS solution was iteratively assessed over a range of plume temperatures to find the best fit to the observed spectrum. Quantification errors due to local variations in the camera-to-pixel distance were suppressed using a subspace projection operator.

Lacking detailed depth-maps for real plumes, the GQ algorithm was tested on synthetic scenes generated by the Digital Imaging and Remote Sensing Image Generation (DIRSIG) software. Initial results showed pixel-by-pixel gas quantification errors of less than 15% for a Freon 134a plume.

**Keywords:** Hyperspectral, longwave infrared, LWIR, thermal band, gas plume, gas quantification, remote sensing

## 1. INTRODUCTION

A chemical plume can occur when an unexpected gas is mixed with the usual effluents of a smokestack. Such plumes, which may be of interest to defence or environmental agencies, are detectable in passive thermal infrared data because they selectively absorb light as it passes through them, and emit light due to their own heat. In 1998, Defence Research and Development Canada (DRDC) Valcartier led the development of the Compact ATmospheric Sounding Interferometer (CATSI) instrument and its GASeous Emission Monitoring (GASEM) detection algorithm, to detect chemical plumes from below. CATSI acquires two sample pixels, angularly separated so that one sample is from the plume and one is from nearby empty sky. By analyzing the difference between the two pixels, GASEM can quantify the amount of gas in the plume with an uncertainty in the order of 15 to 30 percent [1]. With the advent of hyperspectral LWIR imagers, DRDC Valcartier is exploring algorithms for quantifying gas in down-looking imagery.

Compared to up-looking methods, where the background can be reduced to a simple sky model, gas quantification becomes much more challenging when looking down through a plume. Two important complications are:

- The spectrum of ground-leaving radiance varies from pixel to pixel.
- The path-length through the atmosphere varies from pixel to pixel.

There is extensive previous research in hyperspectral gas plume *detection* [3][4], but research into algorithms that *quantify* the gases has been less common. Notable exceptions include Hayden and Noll [5], Gallagher *et al* [6], and Heasler *et al*[7].

* caroline.turcotte@drdc-rddc.gc.ca; phone 1 418 844-4000; fax 1 418 844-4511

Gallagher's approach is particularly interesting. He assumes prior knowledge of plume extent, path radiance, and plume temperature at each pixel, and characterizes the background pixels using either a) basis vectors or b) end-members. In (a) he uses Principal Components Analysis (PCA) to derive basis vectors, and then a generalized least squares (GLS) algorithm to describe each plume pixel with a mixture of basis vectors and plume signatures. In (b) he identifies end-members using a non-negative constrained alternating least-squares algorithm, and then uses an iterative GLS algorithm to describe each plume pixel as a (strictly non-negative) mixture of end-members and plume signatures.

The current "GQ" algorithm extends Gallagher's (b) approach by removing the requirements for prior knowledge, and by providing a new approach to end-member extraction and exploitation. GQ is designed to accept slant path images typically from 8 to 12 μm in a variety of rural or urban backgrounds and any season. Like Gallagher, we use GLS for the final quantification so that a single gas or a gas mixture can be analysed. This paper reviews the development of the gas plume quantification strategy and the corresponding gas quantity accuracy model.

## 2. OVERVIEW OF THE MODEL

Light $L_{plume}$ arriving at a sensor is the sum of the following terms:

$$\vec{L}_{plume} = \vec{L}_{path} + \vec{L}_{terr} \cdot \vec{\tau}_{air} \cdot \vec{\tau}_{plume} + \vec{\tau}_{air} \cdot \left[1 - \vec{\tau}_{plume}\right] \cdot \vec{B}_{plume}\left(T_{plume}\right) \quad (1)$$

where the arrows are included as reminders that each term is spectrally dependant, and:

- $L_{path}$ , $L_{terr}$ = path radiance and ground-leaving radiance;
- $\tau_{air}$, $\tau_{plume}$ = total spectral transmittance of the air (ground-to-camera) and the gas plume;
- $B_{plume}$,( $T_{plume}$ ) = spectrum of a black body at temperature $T_{plume}$

Light $L_{noplume}$ arriving from a non-plume pixel is equal to equation (1) with $\tau_{plume}$ = 1.0. If more than one gas is present, $\tau_{plume}$ must be written as an exponential of the combined absorbances $\alpha_n$. Gas quantization focuses on unmixing the $L_{noplume}$ spectrum and the contributions from the plume:

$$\vec{L}_{plume} = \vec{L}_{noplume} + \tau_{air}\left[B_{plume}\left(T_{plume}\right) - L_{terr}\right] \cdot \left[1 - \exp\left(-\sum \alpha_n C_n\right)\right] \quad (2)$$

where $C_n$ is the amount of gas $n$ in the current pixel [ppm-m] is the parameter of interest. All of the parameters to the right of the equal sign are unknown. GQ uses the following procedure to estimate them:

a. Estimate $L_{noplume}$ by automatically segmentingthe image to identify pixels that represent the same material on the ground. Note that $L_{noplume}$ represents the *at-sensor* radiance that would have been seen if there was no plume, care must be taken to ensure that appropriate atmospheric contributions are included in it.
b. Estimate path transmittance $\tau_{air}$ and radiance $L_{path}$ for the whole scene using an emissivity smoothness algorithm, for exemplars identified in (a).
c. Co-estimate gas abundances $C_n$ , terrain radiances $L_{terr}$, and plume temperature $T_{plume}$ using a generalized least-squares algorithm inside an error minimization algorithm.

The following paragraphs describe these algorithmic steps in more detail.

## 3. EXTRACTING AND CHARACTERIZING END MEMBERS

The analysis of the background terrain is based on the Stochastic Mixing Model (SMM)[8]. The spectra $L_{terr}$ of pixels for a specific end-member are thus modeled using a multi-dimensional Gaussian distribution, characterized by a mean spectrum $\overline{L}$ and a covariance $V$. According to the SMM the probability of a grass pixel spectrum, for example, is:

$$P\left(\vec{L}_{grass}\right) = k \cdot \exp\left[-\frac{1}{2}\left(\vec{L}_{grass} - \overline{L}_{grass}\right)^T V_{grass}^{-1}\left(\vec{L}_{grass} - \overline{L}_{grass}\right)\right] \quad (3)$$

End-members are thus clusters in the $N$-dimensional spectral space. We find them by looking for peaks in a $M$-dimensional histogram of the first $M$ principal components of the full scene[9], as illustrated in Figure 1. The number of dimensions $M$ and the number of bins are scaled in accordance with the image size and the variance and kurtosis of

each principal component band. The histogram must be small enough that large peaks can occur, but large enough to reveal interesting structure in the image. The initial cluster centers of an example DIRSIG scene are illustrated in the figure. Image segmentation is completed by cautiously dilating the clusters along dimensions that simultaneously meet criteria of spatial and spectral proximity, similar to the SPRING algorithm[10]. The mean and variance of the resulting regions of interest (ROIs) in the scene are then suitable for use in the SMM.

.

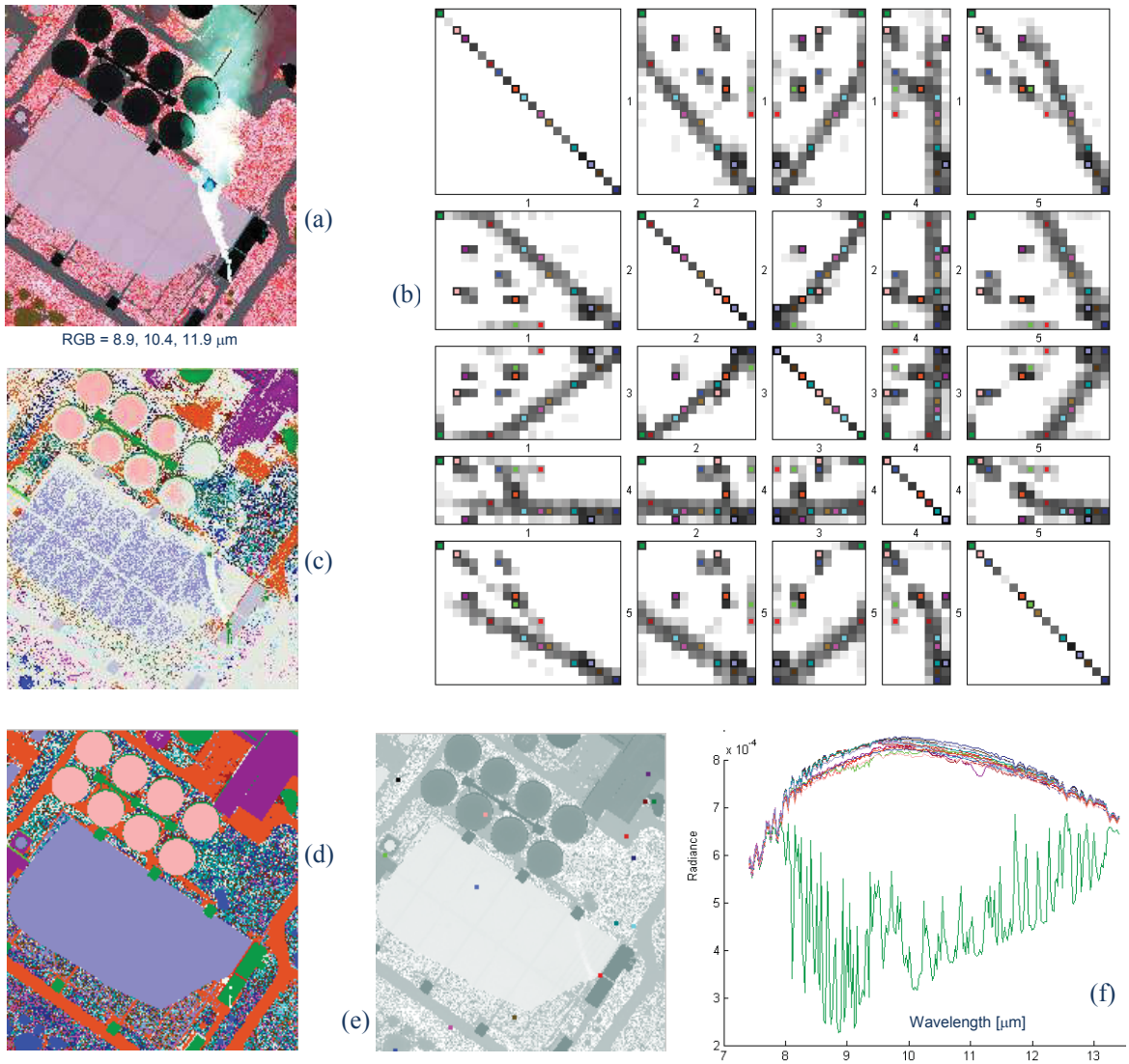


**Figure 1. Automated Image Segmentation and End-Member Extraction**
Starting (a) with a 257-band DIRSIG image, the top 5 principal components are mapped to a 5-dimensional histogram, sketched in (b). Off-diagonal panels in (b) show two-dimensional projections of the histogram, with higher bin-counts shown as darker grey and detected peaks marked in colour. For example in the 1 vs 3 rectangle, the darkness of pixel [*x*,*y*] is proportional to the bin-count over all bins that have those coordinates – "`H(x,:,y,:,:)`" in MATLAB notation. Histogram peaks form the initial ROIs as shown in (c). These ROIs are carefully dilated (d) to complete the segmentation of the image. Single-pixel exemplars (e) from all ROIs have spectra shown in (f). ROI means and covariances are measured for use in the stochastic mixing model. The colour-codes in (b) through (f) identify the corresponding ROIs.

When this algorithm was applied directly to unmodified pixel radiances, it failed to classify pixels within the plume, and it incorrectly extracted separate cluster centers as a function of viewing range. To solve this, the pixel spectra are first projected into a subspace orthogonal[11] to the additive influence of plume and range variations.

## 4. QUANTIFYING ATMOSPHERIC EFFECTS

To solve equation (2), we need path transmittance $\tau_{air}$ and radiance $L_{path}$ for the non-plume atmosphere between the terrain and the camera. Following Thériault[1], we use a simplex optimization algorithm to find the range, air temperature, water vapour, ozone, and ground temperature that imply the spectrally smoothest emissivity curve $\varepsilon_{terr}$ for the terrain:

$$\varepsilon_{terr} = \frac{L_{path} + \tau_{air} L_{sky} - L_{noplume}}{\tau_{air}\left[B_{terr}(T_{terr}) - L_{sky}\right]} \tag{4}$$

where

- $L_{sky}$ = spatially-integrated downwelling radiance at the ground.
- $B_{terr}(T_{terr})$ = spectrum of a black body at the same temperature as the terrain.

GQ does not fit the atmosphere to all pixels in the image (too expensive) nor to the average spectra of the non-plume end-members (averaging might corrupt the signatures) but rather to the selected exemplars of each end-member, as shown in Figure 1(e). The air temperature, water, and ozone values were expected to be constant for all pixels. Figure 2 shows the observed distributions of all five fitted variables.

GQ fits the atmosphere using spectra acquired from calls to MODTRAN 5. To avoid calling MODTRAN for each iteration of the optimization (which would be too slow), GQ creates a locally-linearized "Fast-MODTRAN" model that perturbs "mean" values of $\tau_{air}$ and $L_{path}$ for each new situation, using spectral derivatives from MODTRAN.

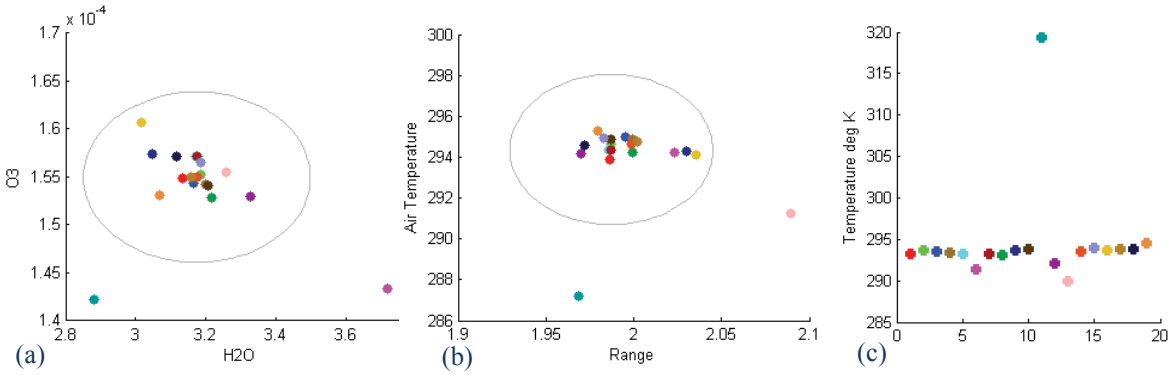


**Figure 2. Estimation of Atmospheric Parameters**
Atmospheric parameters were estimated using the exemplar pixels from all the end-members, as marked by the colours of the dots. Grey circles show two standard deviations around the mean values.

## 5. ADAPTIVE GLS MODEL

For the final step in gas estimation, we linearize Equation 2 in the standard way [6]:

$$1 - \exp\left(-\sum \alpha_n C_n\right) \approx \sum \alpha_n C_n \quad \Rightarrow \quad \vec{L}_{plume} = \vec{L}_{noplume} + \sum C_n Q_n$$
$$\text{where} \quad Q_n = \alpha_n \tau_{air}\left[B_{plume}(T_{plume}) - L_{terr}\right] \cdot \left[1 - \exp\left(-\sum \alpha_n C_n\right)\right] \tag{5}$$

Note that under the stochastic mixing model, $L_{noplume}$ is typically a linear sum of end-members, and hence can be written using the matrix equation shown in Figure 3 (the same matrix expression used by Gallagher *et al* [6]).

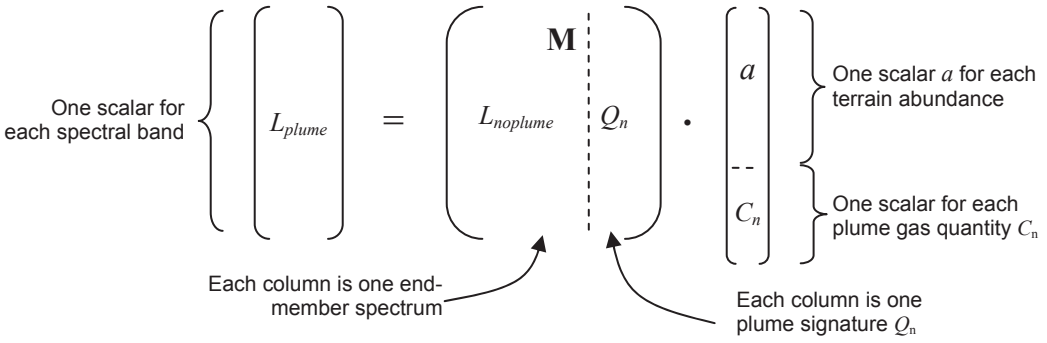


**Figure 3. Matrix Equation for Generalized Least Squares**

Under the stochastic mixing model (3), and assuming that $Q_n$ is well known, the optimal GLS solution to (5) is calculated using the covariance matrix $V$ as follows[12][13]:

$$\begin{bmatrix} \hat{a} \\ \hat{C} \end{bmatrix} = \left(M^T V^{-1} M\right)^{-1} M^T V^{-1} L_{plume} \tag{6}$$

This solution thus finds an optimal combination of terrain materials and plume gases to explain the observed radiance, taking into account that some spectral bands have better signal to noise ratios than others. It is a powerful approach, but it depends for its success on the following four challenging prerequisites:

- It requires a good estimate of the ground-leaving radiance $L_{terr}$, so that $Q_n$ is accurate. Following Gallagher[6], we do this using two or three iterations in which the evolving value of $\hat{a}$ is used to set $L_{terr}$.
- It requires a good estimate of $T_{plume}$, so that $Q_n$ is accurate, as discussed in 5.1.
- It requires an appropriate covariance matrix $V$ that is representative of "normal" spectral variations in ground clutter and plume modeling, as discussed in 5.2
- It requires good knowledge of the pixel-to-camera range, as discussed in 5.3, so that $L_{noplume}$ and $\tau_{air}$ in (5) are calculated correctly.

### 5.1 Estimating the Plume Temperature

GQ estimates the plume temperature using the following iterative technique:

a. Assume a plume temperature;
b. Using equations (5) and (6), find an optimal estimate of what the at-sensor radiance should be;
c. Calculate the mean-square error between the predicted and observed radiances;
d. Repeat (a) through (c) to find the plume temperature that minimizes the mean-square error.

Figure 4 illustrates how the minimum will be sharp in some cases and very shallow in other cases. When the minimum is shallow, there is more uncertainty in the estimated temperature, and hence in the plume concentration.

Field experiments[14] indicate that the difference between plume temperature and ambient air temperature remains constant for a short distance from the stack, and then falls off as the inverse of the distance. This suggests that plume temperatures are locally smooth and thus amenable to spatial interpolation. We plan to experiment with Bayesian interpolation to provide better temperature estimates to pixels where there is no clear fit minimum.

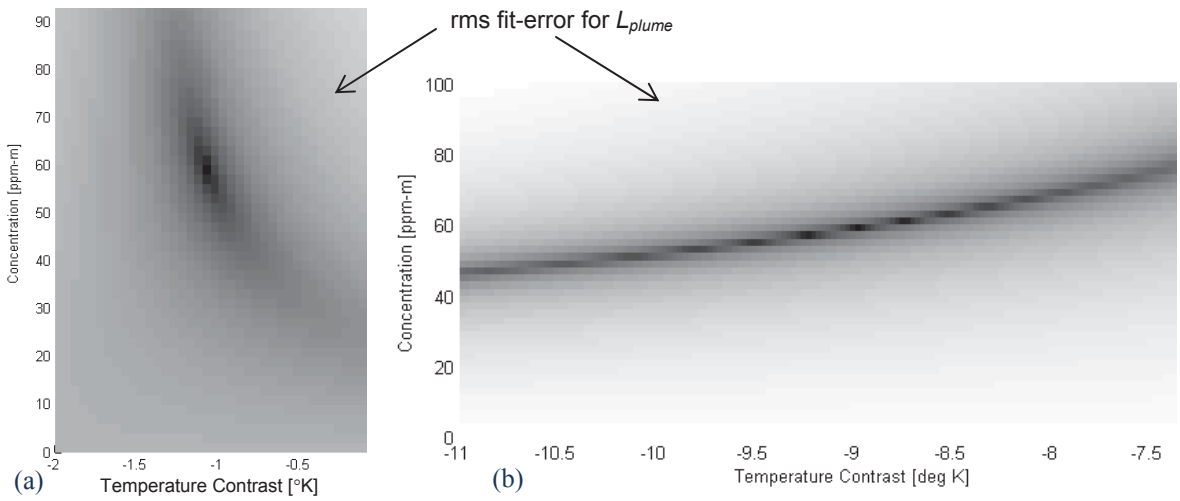


**Figure 4. Challenges Estimating Plume Temperature**
Plume temperature is estimated by minimizing the difference between the predicted and observed radiance $L_{plume}$. In cases such as (a), there is a sharp point of minimum error for 58 ppm-m and a temperature contrast of -1.1°K, and hence no ambiguity about plume concentration. In cases such as (b), there is a long shallow valley, and it may be difficult to tell whether the correct answer is 60 ppm-m or 57 ppm-m. Both these examples show Freon 114 over wetland terrain with gas concentration of 58 ppm-m.

### 5.2 Estimating the Covariance Matrix

The covariance $V$ represents the variability that can be expected in $L_{plume}$, given an ensemble of pixels that all have exactly the same mixture of terrain materials and gas plumes. For a pure pixel will no plume, $V$ is well estimated by the measured covariance in the ROI for that end-member. If there are fewer pixels in the ROI than there are bands, GQ builds $V$ using a Parzen window[15] to avoid problems with low-rank and non-invertible matrices. For pixels that are a mixture of materials, the SMM uses a linear combination of the covariances of the constituent components. Thus for example a pixel that is a mixture of grass and concrete will have $V = a_{grass}\, V_{grass} + a_{cement}\, V_{cement}$[16][17]. If scene-analysis uncertainties (for example in plume temperature estimation) can be expressed as spectral variances, they can also be added to the covariance.

It would be extremely slow, in practice, to re-estimate $V$ and its inverse for every pixel in a plume. GQ therefore speeds up the analysis by treating pixels that were placed in a pure-endmember ROI by the histogram-peak algorithm as pure pixels. For those pixels, only one end-member $L_{noplume}$ is included in the **M** matrix of Figure 3;

### 5.3 Avoiding Errors Due to Unknown Range Variations

The distance from the camera to a ground pixel can change within a scene, due to camera viewing geometry, for example, topographic features, raised structures, or vegetation (see Figure 5). We found that these local variations in range cannot be ignored, because they strongly influence the estimated gas quantity. We solved this by inserting the following subspace projection operator $P$, specifically attuned to changes in the range. The vector $R$ here represents the additive changes in observed radiance $L$, due to a typical uncertainty in range.

$$P = \left(1 - \frac{R \cdot R^T}{R^T \cdot R}\right) \quad \Rightarrow \quad \begin{bmatrix} \hat{a} \\ \hat{C} \end{bmatrix} = \left(M^T P V^{-1} P^T M\right)^{-1} M^T P V^{-1} P^T L_{plume} \tag{7}$$

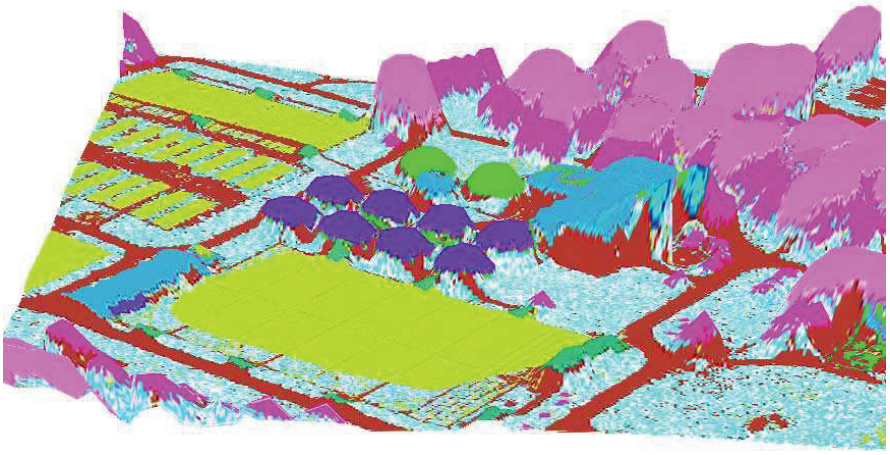

**Figure 5. Variability in Height of Objects in the Scene**
The DIRSIG image shown in Figure 1 is based on a 3-dimensional scene model, rendered here in false colour based on terrain material. A sensor viewing the scene from above therefore sees varying amounts of atmospheric signal from pixel to pixel.

## 6. UNCERTAINTY ESTIMATION

A key objective of the project is to attach accurate error bars to the delivered plume maps. The GLS algorithm provides an appropriate mechanism for doing this, but only if all errors can be mapped to zero-mean spectral uncertainties. For example if there is some uncertainty about the amount of ozone in the air, it will primarily map to spectral uncertainties in the 9-10 μm band. The importance of such an ozone error will depend on whether the gas being detected has a signature in that spectral range.

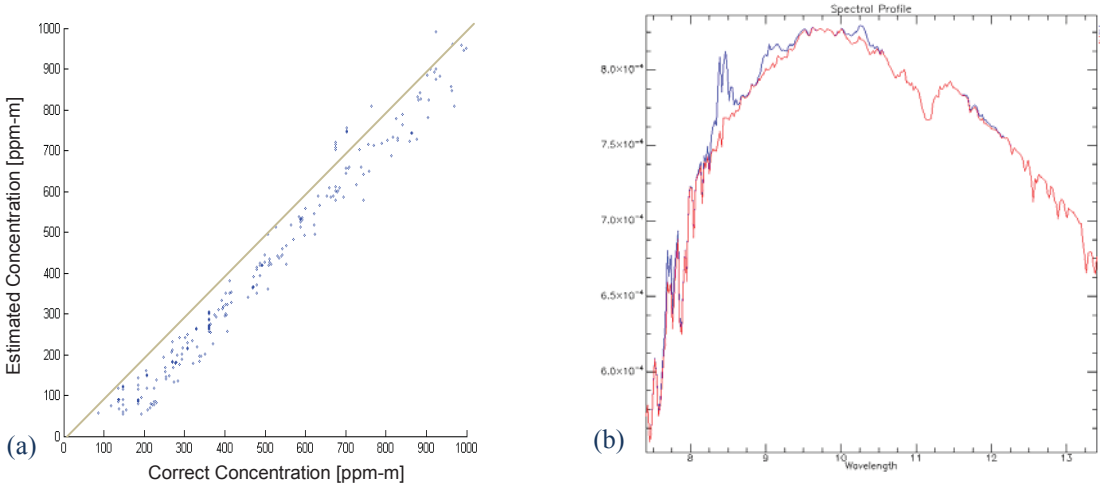


**Figure 6. Initial Quantification Results**
Initial tests with the Freon 134a plume shown in Figure 1a show that the algorithm is correctly estimating plume quantities, though with some bias toward underestimation. Figure (b) shows spectra over the same background and at the same range, with (blue) and without (red) the Freon plume.

GQ's error bar estimation therefore starts with the translation of all known uncertainties into spectral covariances (e.g $V_{o3}$, $V_{range}$, etc.). Uncertainties are forced to be zero-mean by the introduction of offsets where necessary. These

covariances are added into a total covariance $V_{tot}$, and the classification uncertainties for terrain abundances and gas concentration are the found on the diagonal of the following array[12]:

$$E_{rms}^2 = \left(M^T P V_{tot}^{-1} P^T M\right)^{-1} \tag{8}$$

## 7. INITIAL RESULTS

**Error! Reference source not found.** shows initial classification results for the algorithm. Plume quantities are being accurately extracted, though there is some negative bias. Algorithm refinement and further tests with lower gas concentrations are underway.

## REFERENCES


[1] Thériault, AJ.-M., Puckrin, E., "Remote sensing of chemical vapours by differential FTIR radiometry," International Journal of Remote Sensing 26(5), 981-995 (2005).

[2] Rochester Institute of Technology, "DIRSIG, The Digital Imaging and Remote Sensing Image Generation Model," web page at: http://dirsig.cis.rit.edu/ (2008).

[3] Messinger, DW, "Gaseous plume detection in hyperspectral images: a comparison of methods," Proc. SPIE 5425, 592-603 (2004).

[4] Burr, T. and Hengartner, N., "Overview of physical models and statistical approaches for weak gaseous plume detection using passive infrared hyperspectral imagery," Sensors, Vol. 6, 1721-1750 (2006).

[5] Hayden, A. and Noll, R., "Remote trace gas quantification using thermal IT spectroscopy and digital filtering based on principal components of background scene clutter," Proc. SPIE 3071, 158 (1997).

[6] Gallagher, NB., Sheen, DM., Shaver, JM. et al, "Estimation of trace vapor concentration pathlength in plumes for remote sensing applications from hyperspectral images," Proc. SPIE 5093, 184-194 (2003).

[7] Heasler, P., Posse, C., Hylden, J. et al, "Nonlinear Bayesian algorithms for gas plume detection and estimation from hyperspectral thermal image data," Sensors 7, 905-920 (2007).

[8] Stocker, AD. and Schaum, AP., "Application of stochastic mixing models to hyperspectral detection problems," Proc. SPIE 3071, 47-60 (1997).

[9] Silverman, J., Rotman, SR., Caefer, CE., "Segmentation of hyperspectral images from the histograms of principal components," Proc. SPIE 4816, 270-277 (2002).

[10] Espindola, GM., Camara, G., Reis, IA. et al, "Parameter selection for region-growing image segmentation algorithms using spatial autocorrelation," Int. J. Remote Sensing, 27, 12-14, 3035-3040 (2006).

[11] Harsanyi, JC., and Chang, CI., "Hyperspectral image classification and dimensionality reduction: an orthogonal subspace projection approach," IEEE Trans. Geo & Remote Sensing, 32:4, 779-785 (1994).

[12] Kay, SM., [Fundamentals of Statistical Signal Processing: Estimation Theory], Prentice-Hall, New Jersey (1993).

[13] Burr, T., Foy, BR., H. Fry et al., "Characterizing clutter in the context of detecting weak gaseous plumes in hyperspectral imagery," Sensors, vol. 6, 1587-1615 (2006).

[14] Jellison, GP. and Miller, DP, "Validation and calibration of a spectroscopic technique for determination of gas plume temperature," Proc. SPIE 5425, 244-255 (2004).

[15] Theiler, J., Foy, BR., and Fraser, AM., "Characterizing non-Gaussian clutter and detecting weak gaseous plumes in hyperspectral imagery," Proc. SPIE 5806, 182-193 (2005).

[16] Keshava, N., and Mustard, J.F.,, "Spectral unmixing," Signal Processing Magazine, IEEE , v.19, no.1, pp.44-57 (2002).

[17] Boardman, J.W., "Inversion of high spectral resolution data," Proc. SPIE, vol. 1298, pp. 222–233 (1990).